ChemComm

COMMUNICATION

View Article Online
View Journal

Cite this: DOI: 10.1039/d0cc06111e

Received 10th September 2020,
Accepted 21st October 2020

DOI: 10.1039/d0cc06111e

rsc.li/chemcomm

Enhancing photoelectrochemical performance of $ZnIn_2S_4$ by phosphorus doping for sensitive detection of miRNA-155†

Hongyan Liu, * Simin Ai, Yajuan Liu, Hongmei Zeng, Huimei Da, Yaling Liu, Yaqin Chai and Ruo Yuan *

We report the synthesis of phosphorus-doped $ZnIn_2S_4$ ($ZnIn_2S_{4-x}P_x$) materials through a solid/gas-phase reaction. $ZnIn_2S_{4-x}P_x$ shows enhanced photoelectrochemical (PEC) performance due to the improved photo-carrier separation efficiency achieved by substituting some of the sulfur with phosphorus. A PEC biosensor was further developed based on $ZnIn_2S_{4-x}P_x$, which exhibits excellent analytical performance for miRNA-155.

Photoelectrochemical (PEC) bioanalysis is a newly developed analytical technology with higher sensitivity, broader detection ranges, and low-cost instruments.[1–4] The PEC process refers to the conversion of photon-to-current, which is caused by the excitation of photoactive materials and the subsequent charge transfer.[5–7] The photocurrent response efficiency of photoactive materials is a key factor in promoting the performance of PEC biosensors.[8] Therefore, the rational design of photoactive materials is a crucial step in developing high-performance PEC sensors.[9,10]

Bimetallic sulfides, such as $ZnIn_2S_4$, have attracted increasing interest due to their photostability, visible-light absorption, and narrow band gap structure, which are suitable for PEC applications.[11,12] However, the photoelectric conversion efficiency of $ZnIn_2S_4$ is far below what is expected due to the recombination of electrons and holes. Therefore, it is significant to increase the charge separation efficiency of $ZnIn_2S_4$ materials and further enhance their PEC performance. It has been recently reported that introducing defects into photocatalysts can greatly reduce the recombination of electron–hole pairs. The defects could serve as centers to capture the photo-generated electrons and therefore the electron concentration can be manipulated to prevent recombination with the holes.[13–15] For example, vacancy engineering has been employed to improve the photocatalytic activity of the $ZnIn_2S_4$ material. Xie *et al.* found that the introduction of zinc vacancies into $ZnIn_2S_4$ could enhance the carrier transport from the conduction band (CB) to the trap states, accelerate the separation of electrons and holes and also increase the photoabsorption.[16] They also found that substitution of the lattice sulfur atoms of $ZnIn_2S_4$ with oxygen significantly improves the photocatalytic activity, attributed to the fact that the density of states at the valence-band maximum (VB) was increased compared to that of the pristine $ZnIn_2S_4$.[17] Therefore, it is of great significance to explore new dopants to introduce defects that can enhance the charge separation efficiency of $ZnIn_2S_4$. On the other hand, we have noticed that some ternary electrocatalysts of monometallic phosphosulfides, such as CoS|P, MoP|S, and FePS,[18–23] have demonstrated excellent electrocatalytic activity through crossing substitutions between phosphorus and sulfur. Inspired by these metallic phosphosulfides, we propose that the electronic structure of $ZnIn_2S_4$ can be modified by substituting some of the sulfur with phosphorus, and consequently an enhanced photoelectrochemical performance can be expected.

Herein, we demonstrate the design and synthesis of P-doped $ZnIn_2S_4$ ($ZnIn_2S_{4-x}P_x$) through a solid/gas-phase reaction by using NaH_2PO_2 as a P source. A novel "signal off" PEC biosensor for the sensitive detection of the cancer biomarker microRNA-155 was developed based on the $ZnIn_2S_{4-x}P_x$ material. As shown in Scheme 1, $ZnIn_2S_{4-x}P_x$ was immobilized on an electrode to serve as a signal indicator. Hairpin DNA (HP1) was then modified on the electrode, which can be specifically identified by the target microRNA-155. In addition, duplex-specific-nuclease (DSN) enzymes can specifically recognize and digest the DNA portion of the DNA–RNA hybridization chain. The target can then be released for the next cycle. Subsequently, S1-modified SiO_2 nanoparticles can hybridize with the remaining HP1 so that the SiO_2 nanoparticles can be immobilized on the electrode, which can effectively inhibit the electron transfer and a decreased PEC signal can be obtained. Therefore, the photocurrent was quantitatively related to the

Key Laboratory of Luminescence Analysis and Molecular Sensing (Southwest University), Ministry of Education, College of Chemistry and Chemical Engineering, Southwest University, Chongqing 400715, China. E-mail: liuhy860@swu.edu.cn, yuanruo@swu.edu.cn; Fax: +86-23-68253172; Tel: +86-23-68252277

† Electronic supplementary information (ESI) available: Experimental details and electrochemical characterizations. See DOI: 10.1039/d0cc06111e

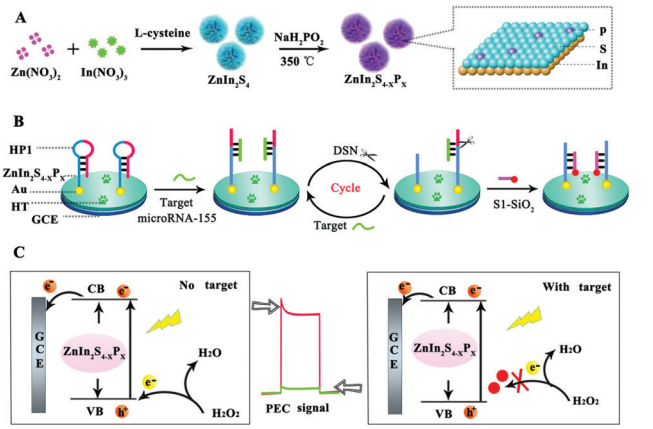

Scheme 1 Schematic illustration for the preparation and mechanism of the PEC biosensor.

concentration of microRNA-155. This PEC biosensor also provided a simple platform for detection of other biomarkers in clinical diagnosis.

The $ZnIn_2S_{4-x}P_x$ material was synthesized by a solid/gas-phase reaction to introduce P into the $ZnIn_2S_4$ structure (see ESI†). Scanning electron microscopy (SEM) was employed to characterize the morphology of the $ZnIn_2S_{4-x}P_x$ material. As shown in Fig. 1A and B, $ZnIn_2S_{4-x}P_x$ shows a flower-like morphology with a diameter of several micrometers. It can be observed that the morphology of $ZnIn_2S_{4-x}P_x$ was similar with that of $ZnIn_2S_4$ (Fig. S1, ESI†). In addition, the elemental mapping of $ZnIn_2S_{4-x}P_x$ indicates the distribution of In, Zn, S and P elements. Obviously, compared with the In and S elements, the weaker density of P implies the low percentage of P in the composite. The powder X-ray diffraction (XRD) pattern of $ZnIn_2S_{4-x}P_x$ shows obvious peaks at $2\theta = 21.6$, 27.5, 47.2, 52.3, and 55.6 (Fig. S2, ESI†), which can be indexed to a hexagonal phase of $ZnIn_2S_4$ (ICDD-JCPDS card No. 72-0773), indicating that the substitution process did not alter the crystal structure of the $ZnIn_2S_4$ material, probably due to the atomic size of P being similar to that of S.

The chemical states and binding environments of $ZnIn_2S_4$ and $ZnIn_2S_{4-x}P_x$ were investigated by using X-ray photoelectron spectroscopy (XPS). The survey spectra of the two composites verified the presence of Zn, In and S, while the peak of P was observed only in the $ZnIn_2S_{4-x}P_x$ sample (Fig. 2A). The high resolution X-ray photoelectron spectroscopy (HR-XPS) regions of Zn 2p, In 3d, S 2p and P 2p are provided in Fig. 2B–E; the binding energy of Zn $2p_{1/2}$ and Zn $2p_{3/2}$ for $ZnIn_2S_4$ was identified at 1044.68 and 1021.61 eV.[24] The two characteristic peaks at 452.03 and 444.49 eV in the spectra of $ZnIn_2S_4$ are ascribed to In $3d_{3/2}$ and In $3d_{5/2}$ while these peaks in the $ZnIn_2S_{4-x}P_x$ sample shifted to 452.28 and 444.69 eV, respectively (Fig. 2C). These positive-shifted peaks after the doping of P imply a strong interaction between P and $ZnIn_2S_4$. The characteristic peaks of P 2p located at 139.57 eV and 133.33 eV for P $2p_{1/2}$ and P $2p_{3/2}$ states were observed in $ZnIn_2S_{4-x}P_x$ (Fig. 2E), suggesting that P is probably incorporated in $ZnIn_2S_4$ by replacing S. The optical absorption properties of the materials were investigated using the UV–vis spectra. As shown in Fig. S3 (ESI†), the results show that the $ZnIn_2S_{4-x}P_x$ samples exhibit higher optical absorption in the visible light region than $ZnIn_2S_4$, indicating that the doping of P increased the optical absorption. Furthermore, the energy band structures of the materials were determined by the XPS valence band (VB) spectra (Fig. 2F). The derived VB maximum of the $ZnIn_2S_4$ and $ZnIn_2S_{4-x}P_x$ samples is about 0.84 and 0.99 eV. It can be clearly observed that the doping of P changed the energy band structure of $ZnIn_2S_4$. The positive-shift of the VB indicates the enhanced oxidation capability, which benefits the oxidation of an electron donor in the PEC system, leading to a higher

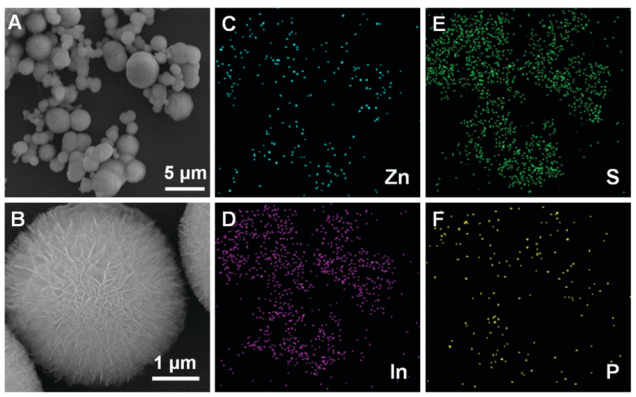

Fig. 1 SEM images of $ZnIn_2S_{4-x}P_x$ (A and B) and EDX energy spectrum of $ZnIn_2S_{4-x}P_x$ (C–F).

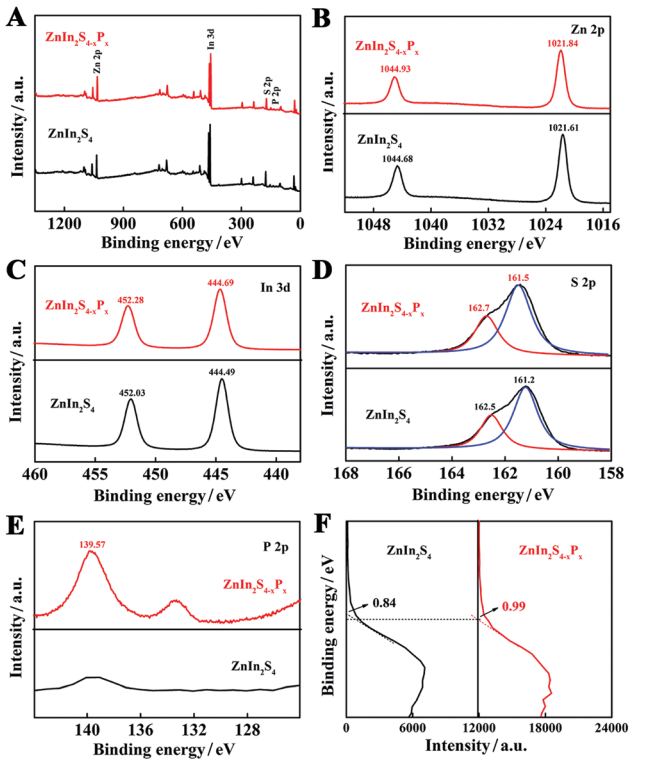

Fig. 2 XPS survey (A), and Zn 2p (B), In 3d (C), S 2p (D), and P 2p (E) spectra of $ZnIn_2S_4$ and $ZnIn_2S_{4-x}P_x$ samples. Valence-band XPS spectra and band structure diagram of $ZnIn_2S_4$ and $ZnIn_2S_{4-x}P_x$ (F).

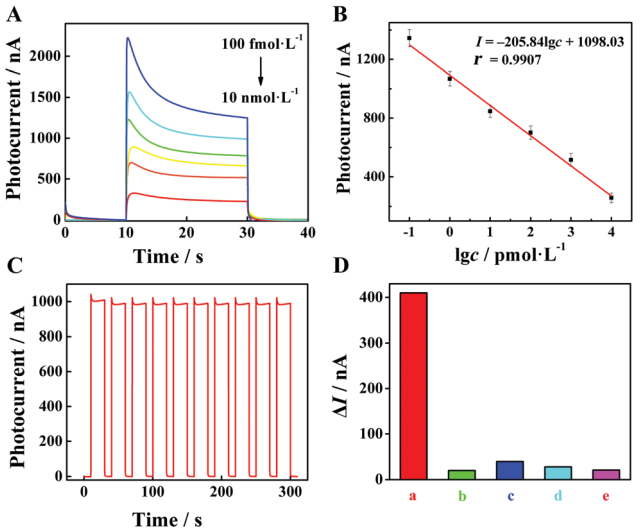

Fig. 3 (A) PEC responses of the biosensors to different concentrations of the target miRNA-155. (B) Corresponding calibration plot for the PEC signal *vs.* lgc. (C) Stability of the PEC biosensor at 1 pM miRNA-155. (D) Selectivity of the PEC miRNA-155 biosensor with a 10-fold excess of other interfering substances (a: miRNA-155, b: miRNA-141, c: miRNA-21, d: miRNA-122, and e: blank).

separation efficiency of carriers, and further results in enhanced PEC performance.

Photoelectrochemical measurements were performed to evaluate the photoelectrochemical performance of $ZnIn_2S_{4-x}P_x$. As displayed in Fig. S4 (ESI†), the photocurrent of $ZnIn_2S_{4-x}P_x$ was 1.3 μA, which was much higher than that of pristine $ZnIn_2S_4$ (0.63 μA). The PEC biosensor was then constructed and characterized by electrochemical impedance spectroscopy (EIS). As shown in Fig. S5A (ESI†), after $ZnIn_2S_{4-x}P_x$ was coated (curve *b*), there was an apparent decrease of the electron transfer resistance (Ret) compared with that of the bare GCE (curve *a*). When the electrode surface was modified with Au NPs, the Ret decreased obviously because of the conductive Au NPs (curve *c*). The Ret successively increased when HP1 (curve *d*), MCH (curve *e*), and miRNA-155 (curve *g*) were incubated on the electrode because the charge transfer was hindered. Additionally, a further increase of the Ret was observed when S1-SiO_2 was incubated on the electrode, suggesting that SiO_2 can further reduce the electron transfer efficiency. PEC characterization was used to investigate the assembly process of the biosensor (Fig. S5B, ESI†). There was no photocurrent of the bare GCE (curve *a*). After $ZnIn_2S_{4-x}P_x$ was coated on the electrode, the initial photocurrent was obtained (curve *b*). When Au NPs were electrodeposited on the electrode (curve *c*), the PEC response was further enhanced because the conductive Au NPs accelerated the electron transfer and thereby the separation of photo-carriers. However, the PEC response continuously declined after HP1 (curve *d*), MCH (curve *e*) and miRNA-155 (curve *g*) were modified on the electrode, owing to the poor electron transfer ability of DNA and MCH. Finally, with the addition of target miRNA-155 and DSN enzymes (curves *f* and *h*), the photocurrent decreased, while an obvious decrease was further observed after S1-SiO_2 was added, due to the fact that SiO_2 can decrease the light absorption of $ZnIn_2S_{4-x}P_x$ and hinder the electron transfer to generate a lower photocurrent.

The analytical performance of the PEC biosensor was further investigated. As shown in Fig. 3A, the PEC signal gradually decreased with the increase of miRNA-155 concentration from 100 fM to 10 nM. The PEC signal intensity and the logarithm of the miRNA-155 concentration showed a good linear correlation in regression equation fitting to $I = -205.84 \log c + 1098.03$, with a detection limit of 33 fM (S/N = 3). The proposed PEC biosensor presented a lower detection limit and wider linear range compared to the reported methodologies (Table S1, ESI†). The stability of the PEC biosensor was a key parameter and investigated by continuous scanning under periodic light irradiation for 10 cycles (Fig. 3C); there was no obvious change of the photocurrent over 10 cycles, indicating that the fabricated PEC biosensor exhibits excellent stability. The selectivity of the PEC sensor was also evaluated. As shown in Fig. 3D, a decrease of photocurrent (ΔI = 410 nA) was observed in the presence of 1 pM miRNA-155. However, there was no obvious decrease of PEC signal in the presence of 10 pM interferences such as miRNA-141, miRNA-21, and miRNA-122. These results indicate that the PEC biosensor has high specificity for the detection of the target miRNA-155.

In conclusion, a novel "signal off" PEC biosensor was developed based on the $ZnIn_2S_{4-x}P_x$ photoactive material. By using NaH_2PO_2 as the P precursor, defective $ZnIn_2S_{4-x}P_x$ was synthesized by a solid/gas phase reaction. The PEC performance of the photoactive $ZnIn_2S_{4-x}P_x$ was remarkably enhanced, which was attributed to the improved photo-carrier separation efficiency achieved by the defects introduced by substituting some of the sulfur with phosphorus. The fabricated PEC biosensor shows high specificity, stability and a broad detection range for the detection of miRNA-155. We believe that this novel PEC platform can be extended to the easy detection of other targets in bioanalysis.

This work was financially supported by the Chongqing Research Program of Basic Research and Frontier Technology (cstc2020jcyj-msxmX0386) and the National Natural Science Foundation of China (21501081).

Conflicts of interest

The authors declare no competing financial interest.

Notes and references

1 W. W. Zhao, J. J. Xu and H. Y. Chen, *Chem. Rev.*, 2014, **114**, 7421–7441.
2 L. T. Huang, J. L. Chen, Z. H. Yu and D. P. Tang, *Anal. Chem.*, 2020, **92**, 2809–2814.
3 H. B. Li, Y. L. Li, J. Li, F. Yang, L. Q. Xu, W. Wang, X. X. Yao and Y. D. Yin, *Anal. Chem.*, 2020, **92**, 4094–4100.
4 Z. Z. Li, C. J. Su, D. Wu and Z. H. Zhang, *Anal. Chem.*, 2018, **90**, 961–967.
5 Q. Zhou, G. H. Li, K. Y. Chen, H. Yang, M. R. Yang, Y. Y. Zhang, Y. K. Wan, Y. F. Shen and Y. J. Zhang, *Anal. Chem.*, 2020, **92**, 983–990.
6 F. Z. Chen, D. M. Han and H. Y. Chen, *Anal. Chem.*, 2020, **92**(12), 8450–8458.

7 Q. Hao, X. N. Shan, J. P. Lei, Y. Zang, Q. H. Yang and H. X. Ju, *Chem. Sci.*, 2016, **7**, 774–780.
8 J. Shu and D. P. Tang, *Anal. Chem.*, 2020, **92**, 363–377.
9 Y. M. Fu, K. Zou, M. Y. Liu, X. H. Zhang, C. C. Du and J. H. Chen, *Anal. Chem.*, 2020, **92**, 1189–1196.
10 W. W. Zhao, J. J. Xu and H. Y. Chen, *Anal. Chem.*, 2018, **90**, 615–627.
11 S. Q. Zhang, X. Liu, C. B. Liu, S. L. Luo, L. L. Wang, T. Cai, Y. X. Zeng, J. L. Yuan, W. Y. Dong, Y. Pei and Y. T. Liu, *ACS Nano*, 2018, **12**, 751–758.
12 H. Liu, J. Zhang and D. Ao, *Appl. Catal., B*, 2018, **221**, 433–442.
13 Q. C. Wang, Y. P. Lei, D. S. Wang and Y. D. Li, *Energy Environ. Sci.*, 2019, **12**, 1730–1750.
14 J. Di, J. Xia, M. F. Chisholm, J. Zhong, C. Chen, X. Cao, F. Dong, Z. Chi, H. Chen, Y. X. Weng, J. Xiong, S. Z. Yang, H. Li, Z. Liu and S. Dai, *Adv. Mater.*, 2019, **31**, 1807576.
15 C. L. Teng, F. Yang, M. H. Sun, K. S. Yin, Q. T. Huang, G. Y. Fu, C. Q. Zhang, X. H. Lu and J. X. Jiang, *Chem. Sci.*, 2019, **10**, 7600–7609.
16 W. L. Yang, L. Zhang, J. F. Xie, X. D. Zhang, Q. H. Liu, T. Yao, S. Q. Wei, Q. Zhang and Y. Xie, *Angew. Chem., Int. Ed.*, 2016, **55**, 6716–6720.
17 X. C. Jiao, Z. W. Chen, X. D. Li, Y. F. Sun, S. Gao, W. S. Yan, C. M. Wang, Q. Zhang, Y. Lin, Y. Luo and Y. Xie, *J. Am. Chem. Soc.*, 2017, **139**, 7586–7594.
18 M. C. Acevedo, M. L. Stone, J. R. Schmidt, J. G. Thomas, Q. Ding, H. C. Chang, M. L. Tasi, J. H. He and S. Jin, *Nat. Mater.*, 2015, **14**, 1245–1251.
19 X. Long, G. X. Li, Z. L. Wang, H. Y. Zhu, T. Zhang, S. Xiao, W. Y. Guo and S. H. Yang, *J. Am. Chem. Soc.*, 2015, **137**, 11900–11903.
20 W. Liu, E. Y. Hu, H. Jiang, Y. J. Xiang, Z. Weng, M. Li, Q. Fan, X. Q. Yu, E. I. Altman and H. L. Wang, *Nat. Commun.*, 2016, **7**, 10771.
21 D. Mukherjee, P. M. Austeria and S. Sampath, *ACS Energy Lett.*, 2016, **1**, 367–372.
22 J. Kibsgaard and T. F. Jaramillo, *Angew. Chem., Int. Ed.*, 2014, **53**, 14433–14437.
23 Y. Hou, M. Qiu, T. Zhang, X. D. Zhuang, C. S. Kim, C. Yuan and X. L. Feng, *Adv. Mater.*, 2017, 1701589.
24 J. Qiu, M. Li, L. Yang and J. Yao, *Chem. Eng. J.*, 2019, **375**, 121990.

